*P. Pilvin**

The Contribution of Micromechanical Approaches to the Modelling of Inelastic Behaviour of Polycrystals

REFERENCE Pilvin, P., **The contribution of micromechanical approaches to the modelling of inelastic behaviour of polycrystals,** *Multiaxial Fatigue and Design*, ESIS 21 (Edited by A. Pineau, G. Cailletaud and T. C. Lindley) 1996, Mechanical Engineering Publications, London, pp. 3–19.

ABSTRACT The purpose of this paper is to make an evaluation of mathematical constitutive equations devoted to the mechanical description of some specific effects observed in metallic polycrystals submitted to multiaxial and/or cyclic loading paths (ratchetting, overstrengthening). Two approaches are analysed: (i) the first one is the issue of an inductive method essentially based on a phenomenological analysis of experimental results; (ii) the second is the outcome of a more deductive process with models able to use/provide information on the microstructure. It will be shown that all of these specific effects can be easily described with a polycrystalline approach based on a simple representation of the microstructure of the material: orientation distribution function and slip systems. The model used is applied to the simulation of yield surfaces, ratchetting phenomena and overstrengthening effect for FCC alloys.

1 Introduction

A great number of proposals have been made during the last twenty years for the mathematical description of the mechanical behaviour of metallic polycrystals. Two approaches may be distinguished. In the first one, the representative volume element is considered as a 'black box'. Consequently, the development of this kind of constitutive equation is mainly based on a phenomenological analysis of experimental results. In these models, all the variables used are defined on a macroscopic scale and the thermodynamical concept of internal state variables is frequently invoked. The main disadvantage of this approach is the lack of predictive character, the use of the model being limited to the domain covered by the experimental datebase. In the second approach, a more deductive process is considered in order to take into account any kind of microstructural information on the material. Pertinent scales have to be introduced to model elementary mechanisms of the inelastic deformation. In these models, the introduction of a 'quasiphysical' description naturally leads to increasing the modelling capabilities. On the other hand, the constitutive equations obtained with the second approach have a large number of

*Université Pierre et Marie Curie and Centre des Matériaux, Ecole des Mines de Paris, URA CNRS 866, BP87, 91003 Evry Cedex, France.

variables (typically between 200 and 10 000). At the present time, this disadvantage limits the use of these models in structural mechanics codes but the increase of computational power and the developments of parallel architectures would allow a broader use.

In Section 2, a short review of the classical models coming from the inductive approach is given. Only unified viscoplastic formulations (one variable to describe the inelastic strain) are considered here. The validity domain of these models under cyclic multiaxial loading is then appreciated. Section 3 is devoted to a brief presentation of the polycrystalline models, and its possible contribution to the development of the inductive approach is evaluated. Finally, these two approaches will be compared with a set of experimental data including specific effects observed in metallic polycrystals submitted to multiaxial and/or cyclic loading paths (ratchetting phenomena, overstrengthening effect).

2 The Inductive Approaches

As the development of these constitutive equations is mainly based on a phenomenological analysis, the fundamental experimental results associated to these models are briefly recalled. In these models, 'internal variables' are introduced to describe the present state and predict the evolution. If there are some attempts to justify, from a metallurgical point of view, the choice and the nature of these internal variables, it should be observed that all these variables are only defined at a macroscopic scale. Consequently, they act as a volume averaged representation of the microstructural mechanisms.

2.1 *Modelling of elastic domain*

The description of the metallic materials behaviour in the inelastic range requires, at first, to specify the evolution of the elasticity domain with respect to the hardening state of the material. As shown later, this step is fundamental as long as it strongly influences the plastic flow rules and the evolution laws of the internal variables. With an inductive approach, this modelling is based on experimental facts. Many experiments are carried out to determine the initial shape and the evolution of the elastic domain (**1, 2**). At the present time, the experimental devices are limited to characterizing plane cross-sections of the domain through biaxial tests. The usual technique consists in carrying out tests on thin-walled circular tubes with tension/compression–torsion or tension/compression–internal pressure loading. The analysis of such results shows that the elastic domain modifications due to hardening are significant and rather difficult to describe. Nevertheless, it is possible to split these modifications into three components:

(1) a translation;
(2) an expansion or a contraction of the domain size;
(3) a distortion with respect to the initial shape of elastic domain.

For the sake of simplicity, the classical constitutive equations assume that the modelling of the current elastic domain could be defined with two transformations only: a similarity and a translation. The similarity allows the description of the expansion (or contraction) of the initial domain and is associated with isotropic hardening effects (R). The translation is associated with kinematic hardening effects (X), and relates to local strain incompatibilities. The distortion of the current elastic domain is therefore not taken into account in classical models. In the framework of initially isotropic materials, the boundary of the current elastic domain can be described by the following expression, for pressure independent plasticity

$$F(\boldsymbol{\Sigma}, R, \mathbf{X}) = \bar{\Sigma}(\boldsymbol{\Sigma} - \mathbf{X}) - R - R_0 + G(R, \mathbf{X}) = 0 \tag{1}$$

where $\boldsymbol{\Sigma}$ stands for the macroscopic stress tensor, and $\bar{\Sigma}$ is a stress homogeneous function of the two invariants of the deviator of $(\boldsymbol{\Sigma} - \mathbf{X})$. In most of the models, the function $G(R, \mathbf{X})$ is equal to zero. Nevertheless its incorporation is needed to integrate nonlinear hardening rules in the framework of 'generalized standard materials' (3). It should be observed that the choice of a particular shape to describe the evolution of the elastic domain is probably the most important step in the model elaboration. In fact, the choice of an *a priori* explicit form for the function $\bar{\Sigma}$, frequently deduced from the initial shape of the elastic domain, is very restrictive because the shape of the current yield surface remains unchanged during the whole history. Recent propositions have thus introduced an implicit form for the description of the shape of the elastic domain, thereby allowing more flexibility for its evolution (4).

2.2 *Evolution laws for internal variables*

In the inductive approach, the choice of the number of internal variables, of their type and their evolution law is based on experimental results. Of course, this is consistent with the methodology, but frequently the tests are performed under one-dimensional loading, so that the question of the extrapolation of these equations – which essentially contain one-dimensional information – to three-dimensional situations can be addressed. The model developed at ONERA (5) is one of the most popular unified constitutive equations. Its hierarchical structure based on the superposition of several variables to describe the kinematic and isotropic hardening effects leads to a fairly good representation of experimental results under proportional loading paths. The equations of this model (summarized below) have enough ingredients (5) to meet with other unified theories (6, 7, 8) and can therefore be used as a reference model. In the present paper, it was decided to present the structure of these constitutive equations in the framework of the thermodynamics of irreversible process (9). The quadratic terms $G(R_i, \mathbf{X}_j)$ introduced in the yield function F allow to find the nonlinear kinematic hardening rule proposed by Armstrong and Frederick for ($\bar{X}_j = 0$, $C_j > 0$ and $D_j > 0$) and the isotropic hardening rule proposed by

Voce for ($R_i = 0$, $b_i > 0$ and $Q_i > 0$). The function $\Omega_2(R, \mathbf{X})$ accounts for time recovery effects for each hardening variable. The evolution laws obtained here, equation (2d), are then a generalized standard version of the ONERA model (**10**). The original constitutive equations (**5**) can be found by using, in equation (2d), the viscoplastic 'multiplier' $\Omega_1'(F-G)$ instead of $\Omega_1'(F)$. These equations can also be used for time-independent plasticity with $\Omega_2 = 0$, using the 'characteristic function' of F for Ω_1. Below are summarized the unified constitutive equations:

State laws (internal variables: $\mathbf{E}^p$, q_i, $\boldsymbol{\alpha}_j$).

$$\boldsymbol{\Sigma} = 2\mu\left\{\mathbf{I} + \frac{\nu}{1-2\nu}\,1 \otimes 1\right\}\mathbf{E}^e \tag{2a}$$

$$R_i = b_i Q_i q_i \quad \text{with} \quad R = \underset{i \in I}{\text{Sum}}\,(R_i) \tag{2b}$$

$$\mathbf{X}_j = \frac{2}{3} C_j \boldsymbol{\alpha}_j \quad \text{with} \quad \mathbf{X} = \underset{j \in J}{\text{Sum}}\,(\mathbf{X}_j) \tag{2c}$$

Evolution laws.

$$-\dot{\mathbf{E}}^p = \frac{\partial \Omega}{\partial(-\boldsymbol{\Sigma})}; \quad -\dot{q}_i = \frac{\partial \Omega}{\partial R_i}; \quad -\dot{\boldsymbol{\alpha}}_j = \frac{\partial \Omega}{\partial \mathbf{X}_j}$$

$$\Omega(\boldsymbol{\Sigma}, R, \mathbf{X}) = \Omega_1(F) + \Omega_2(R_i, \mathbf{X}_j); \quad \Omega_1(F) = \frac{K}{n+1}\left[\frac{\text{Max}(0, F)}{K}\right]^{n+1}$$

$$F(\boldsymbol{\Sigma}, R, \mathbf{X}) = J_2(\boldsymbol{\Sigma}^d - \mathbf{X}^d) - R - R_0 + G(R_i, \mathbf{X}_j) \quad \text{with} \quad J_2(\cdot) = \sqrt{\frac{3}{2}\,\text{Tr}(\cdot^2)}$$

$$G(R_i, \mathbf{X}_j) = \frac{1}{2}\,\underset{i \in I}{\text{Sum}}\,\frac{1}{Q_i}\,[\text{Max}(0, |R_i| - \bar{R}_i)]^2 + \frac{1}{2}\,\underset{j \in J}{\text{Sum}}\,\frac{D_j}{C_j}\,[\text{Max}(0, J_2(\mathbf{X}_j) - \bar{X}_j)]^2 \tag{2d}$$

The numerical simulations show that, for one-dimensional loading, two correlated phenomena are still not correctly represented with this kind of model: the mean stress relaxation and the progressive strain accumulation when the cyclic loading has a non-zero mean value. This inadequacy is well known and recent proposals (introduction of a threshold $\bar{X}_j$ in the dynamic recovery term and significant increase of the number of kinematic hardening variables) clearly improve the predictions of the original model (**11**, **12**).

The important development of biaxial testing has led to a large number of modifications in order to improve agreement with experimental results, and to get expanded multiaxial applicability. The overstrengthening effect under non-proportional loading path is an example of such a phenomenon, observed

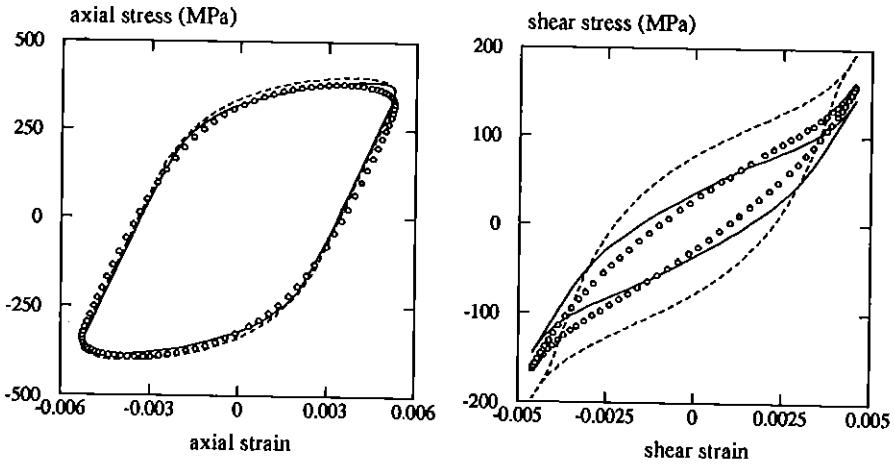

Fig 1 Stress–strain curves for a tension/torsion test on 316L stainless steel at R.T. under non-proportional loading path defined by $E_{11} = \varepsilon_0 \sin\{\omega t\}$ and $2E_{12} = \lambda\sqrt{3}\varepsilon_0 \sin\{\omega t - \phi\}$ with ($\lambda = 0.5$, $\phi = 33°$). Symbols (○): experimental data from (15); dashed lines: classical modelling.

for several alloys in the early 1980s (**13, 14, 15**), for which recent modifications were made in the model (**14, 15**). Most of these improvements introduced a measure of the loading non-proportionality and a modification of the isotropic hardening rules. Several proposals are reported in previous papers, but, even if these modifications allow to reach the observed extra-hardening effect, they also produce a shape of the hysteresis loops which does not agree with experiments. As illustrated in Fig. 1, this anomaly is present for 316L stainless steel loaded at room temperature in tension/compression–torsion ($\Sigma_{11} = \varepsilon_0 \sin\{\omega t\}$ and $2\Sigma_{12} = \lambda\sqrt{3}\varepsilon_0 \sin\{\omega t - \phi\}$) with a small phase lag ($\lambda = 0.5$, $\phi = 33°$) (**15**). With the model used (**15**), the hysteresis loop is in good agreement with experimental data for the axial component, but the loop corresponding to the shear components is too open. This defect results from yield surface distortion which is not represented in the model.

3 The Deductive Approaches

This part is devoted to the presentation of some models built in the framework of the deductive approach, using a simplified description of the microstructure. As a first step, the general methodology applied to metallic polycrystals is shown. The model chosen for the numerical simulation of the experimental database is then written in a more detailed way.

3.1 *The classical polycrystalline models*

The heterogeneity of the material element on a micro-scale is introduced in the model, together with the representation of the elementary deformation mech-

anisms. A good knowledge of the microstructure is then needed, and the main difficulty arising with this type of approach is the choice of the pertinent scale and of the critical mechanisms. In the specific case of metallic materials, a crude description is currently used: even after large advances in physics of solids, the atomic level remains unreachable if the final goal of the description is to perform macroscopic simulations in a reasonable CPU time. It follows that the dislocations cannot be directly represented. The effectiveness of the models is nevertheless related to the description of the various heterogeneity levels. For most of the models, one level is considered: the grain. They are developed to be applied in finite transformations, under monotonic loading, their purpose being generally to determine the shape of the yield surface or to predict texture evolution. The uniformity of the mechanical fields (stress and strain) is assumed in each phase. It is noted here that a 'phase' is only defined from a geometrical point of view through the crystallographic orientation, and not by the morphology or the relative position of one grain with respect to the other (no size effect, no neighbourhood effect).

For a 'grain', the modelling of the material deformation is generally restricted to the effect of crystallographic slip. The behaviour is defined by the generalized Schmid law, which assumes that a slip system is active when its shear stress reaches a critical value. The description of the hardening is then introduced at this level, provided the value of this critical shear stress on each slip system depends on hardening variables. 'Latent hardening' is present if the value computed for a given system is related to the values of the other systems. The plastic strain rate $\boldsymbol{\varepsilon}^p$ of a grain is classically obtained from the knowledge of all the shear strain rates $\dot{\gamma}_s$ on each slip system:

$$\dot{\boldsymbol{\varepsilon}}^p = \underset{s \in S}{\text{Sum}} \left(\mathbf{m}_s \dot{\gamma}_s\right) \quad \text{with} \quad \mathbf{m}_s = \frac{1}{2}\left[n_s \otimes l_s + l_s \otimes n_s\right] \tag{3}$$

In the previous expression, $\mathbf{m}_s$ characterizes the orientation of the slip system defined by the unit vector n_s, normal to the slip plane, and the unit vector l_s, giving the slip direction.

The calculation of the resolved shear stress for the slip system can also be expressed as a function of the local stress in the grain $\boldsymbol{\sigma}$, by means of the same tensor, as $\tau_s = \boldsymbol{\sigma} : \mathbf{m}_s$. The definition of the mechanical behaviour on the elementary level is completed by the evolution rules for transgranular variables, and especially γ_s. A number of theories can be found in the literature. The simplest ones use crystallographic slip as hardening variable (16). More complex solutions introduce variables associated with dislocation density (17, 18). An alternative solution consists in introducing at this level a kinematic hardening variable. The purpose of this choice is to take account of the local heterogeneities inside of the grain, which are not modelled in expression (3), as γ_s stands for the mean value of plastic slip in the grain. This method, adapted from the inductive approach (19), seems to be questionable, but it represents a pragmatic

solution to describe with a low number of variables the transgranular heterogeneity, even if that can also be made by following other approaches (**20**).

The final aspect of the polycrystalline model is the definition of the relations between the variables in each grain of the aggregate (σ, ε, ε^p) and the global macroscopic variables ($\mathbf{\Sigma}$, $\mathbf{E}$, $\mathbf{E}^p$). The self-consistent approach is a good tool to represent the grain-to-grain interaction (**21**). The one-site approaches compute the stress in phase, which individual behaviour is known, as the result of the calculation on an ellipsoidal inclusion in an homogeneous equivalent continuum. They permit greater precision in the assumptions (sometimes implicit assumptions) made in other interaction models. In the simple case of a global and local isotropic continuum, the global inelastic strain is the average of the local inelastic strains, so that the following relation can be *a priori* expressed

$$\sigma = \mathbf{\Sigma} + a\mu(\mathbf{E}^p - \varepsilon^p). \tag{4}$$

This equation represents a model with uniform stress ($a = 0$) (**22**), Lin-Taylor's model ($a = 2$) (**23**), or Kröner's model, with an elastic accommodation ($a \approx 1$) (**24**). From a practical point of view, this expression is often used with lower 'a' values (constant values lying between 0.01 and 0.2 (**25**, **19**, **18**), the elastic accommodation overestimating the intergranular stresses (**26**). The evaluation of the correct form of the elastoplastic accommodation has been made by Hill (**27**) for time-independent plasticity, but the numerical treatment of the resulting implicit integral equation is not simple. A simplification, valid for proportional loading, has been proposed (**28**): in expression (4), the shear modulus is replaced by the secant elastoplastic modulus (with $a = 1$). This modification may have a strong influence, especially for the case of small perturbations.

3.2 *The polycrystalline model used*

The model which has been used for the material identification is a new release of the initial version due to Cailletaud (**29**). The formulation of the model on the local level is made in the framework of viscoplasticity, in order to improve the efficiency of the numerical treatment. This classical choice allows to directly compute the shear strain rate from the actual value of the resolved shear stress and of the internal variables. Nevertheless, with suitable values of the viscosity coefficients (k and n), the global behaviour becomes time-insensitive. The main specificity of the model is the introduction of transgranular variables able to model the cyclic behaviour. The set of equations of the polycrystalline model is presented below. The localization relation, equation (5a), is given *a priori* under an explicit form. It involves a supplementary variable for each phase, β^g, allowing the intergranular stresses to be relaxed. The value of the coefficient, a, may remain of the order of unity, so that the model reduces to Kroner's model on the onset of viscoplastic flow. The fading memory term in equation (5h) produces an accommodation of the intergranular incompatibilities, the rule of which is similar with Zaoui–Berveiller's (**28**), for monotonic loading. Two

hardening variables are introduced for each mechanism. The latent hardening, which is correlated with overstrengthening associated to nonproportional loading, is modelled by an isotropic variable r_s, and an interaction matrix h_{rs}. The kinematic hardening variable x_s accounts for the local heterogeneities inside the grain; a possibility of time recovery is introduced for this variable, equation (5f).

Localization rule

$$\boldsymbol{\sigma} = \boldsymbol{\Sigma} + a\mu[\mathbf{B} - \boldsymbol{\beta}^g]; \ \mathbf{B} = \underset{g \in G}{\text{Sum}} (f_g \boldsymbol{\beta}^g) \tag{5a}$$

Constitutive equations for each phase

$$\tau_s = \boldsymbol{\sigma} : \mathbf{m}_s; \ x_s = c\alpha_s; \ r_s = Q_1 \underset{r \in S}{\text{Sum}} (h_{rs} q_r) + Q_2 \rho_s \tag{5b}$$

$$F_s = |\tau_s - x_s| - r_0 - r_s + G_s; \ G_s = \frac{1}{2}\frac{d}{c} x_s^2 \tag{5c}$$

$$\dot{\gamma}_s = \left[\text{Max}\left\{0; \frac{F_s \text{ or } F_s - G_s}{k}\right\} \right]^n \text{Sign}(\tau_s - x_s) \tag{5d}$$

$$\dot{q}_s = |\dot{\gamma}_s|(1 - b_1 q_s); \ \dot{\rho}_s = |\dot{\gamma}_s|(1 - b_2 \rho_s) \tag{5e}$$

$$\dot{\alpha}_s = \dot{\gamma}_s - d\alpha_s |\dot{\gamma}_s| - \left\{\frac{|x_s|}{M}\right\}^m \text{Sign}(x_s) \tag{5f}$$

$$\dot{\boldsymbol{\varepsilon}}^p = \underset{s \in S}{\text{Sum}} (\mathbf{m}_s \dot{\gamma}_s) \tag{5g}$$

$$\dot{\boldsymbol{\beta}}^g = \dot{\boldsymbol{\varepsilon}}^p - D\{\boldsymbol{\beta}^g - \delta \boldsymbol{\varepsilon}^p\} \frac{2}{3} J_2(\dot{\boldsymbol{\varepsilon}}^p) \tag{5h}$$

Homogenization

$$\mathbf{E}^p = \underset{g \in G}{\text{Sum}} (f_g \boldsymbol{\varepsilon}^p); \ \mathbf{E}^e = \frac{1}{2\mu}\left\{\mathbf{I} - \frac{\nu}{1+\nu}\mathbf{I} \otimes \mathbf{I}\right\}\boldsymbol{\Sigma} \tag{5i}$$

3.3 *The capabilities of the polycrystalline approaches*

The purpose of this section is to illustrate the capabilities of the polycrystalline approaches on FCC polycrystals, for which the predominant deformation mechanism is the crystallographic slip on the octahedral systems $\{111\}\langle 110\rangle$. For each new material, the computations are performed by using the orientation distribution function, taken under a discrete form. If this information is missing, an isotropic distribution is chosen. It is made from 40 equivalent orientations ($\forall g \in G; f_g = 1/40$) (**30**).

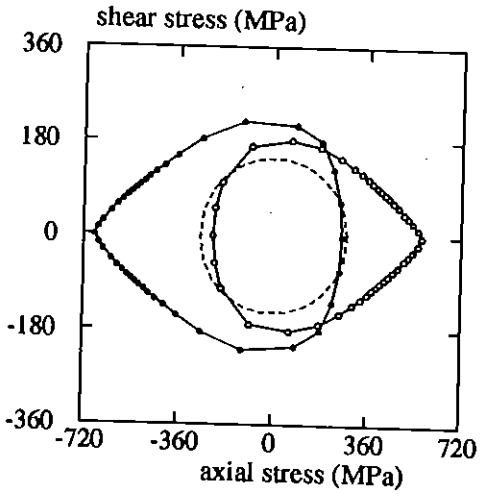

Fig 2 Simulation of the distortion of the yield surface with the polycrystalline model under tension–compression loading (the initial yield surface is plotted with broken lines).

As a key point of this model type, it can be checked that the equations naturally predict a good description of the evolution of the elastic domain (**19, 30**), specially the distortion of the yield surface. This fact is illustrated in Fig. 2 under a tension-compression loading. The property is confirmed in Fig. 1, where the micromechanical model gives a good description of the hysteresis loop for the shear components, due to the rapid rotation of the normal characterizing

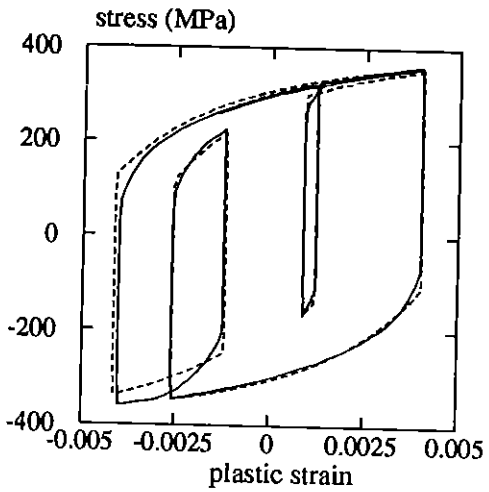

Fig 3 Simulations of small strain cycles in a large one with both models.

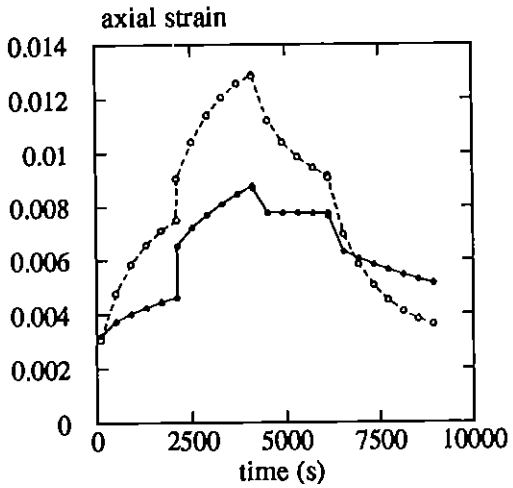

Fig 4 Simulations of one-dimensional ratchetting test with both models: 5 cycles (+330/−270 MPa), 5 cycles (+360/−240 MPa), 5 cycles (+330/−270 MPa) and 5 cycles (+300/−300 MPa).

the plastic flow: this movement is made possible by the fact that a corner develops on the vicinity of the actual loading point.

The effect of latent hardening naturally produces a good description of the overstrengthening effect, as previously shown on 316L stainless steel (29), for Waspaloy and an aluminium alloy (31).

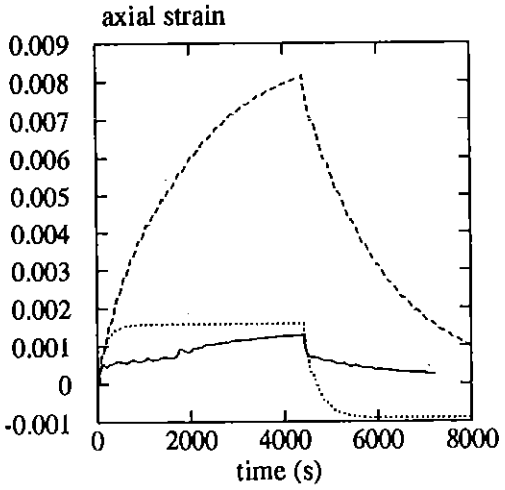

Fig 5 Simulations of two-dimensional ratchetting test with both models: 5 cycles ($\Sigma_{11} = 50$ MPa and $E_{12} = \pm 0.4\%$), 5 cycles ($\Sigma_{11} = 50$ MPa, $E_{12} = \pm 0.7\%$) and 5 cycles ($\Sigma_{11} = 0$ MPa, $E_{12} = \pm 0.7\%$)].

Last, but not least, the multicriteria character of this approach produces good qualitative predictions of the ratchetting phenomenon. For instance, Fig. 3 shows that a small cycle remains 'suspended' in a large one, which is an essential feature to predict ratchetting under one-dimensional loading (**32**). Figures 4 and 5 illustrate the good qualitative agreement of the approach for one-dimensional and two-dimensional ratchetting tests, compared with classical models. Note that Figs. 1, 3, 4 and 5 have been performed for the classical model (dashed lines), with the coefficients given in Table 1 (E = 180 GPa, $\nu = 0.33$), and, for the polycrystalline model (solid lines), with the coefficients given in Table 2 (with $a = 1$), using $h_{rs} = 1$ for the interaction matrix, except the coefficient corresponding to the Lomer–Cotrell interactions, denoted by h_{LC}, whose value is 1.46. The simulation of the biaxial ratchetting test has also be performed with a macroscopic kinematic rule, equation (6), specially designed to reduce the ratchetting effect (**33**).

Table 1 Coefficients of the classical model used for the simulations (units: MPa s)

Material	R_0	Q_1	b_1	C_1	D_1	$\bar{X}_1$	C_2	D_2	$\bar{X}_2$	K	n
A 316L	188	0	32	45900	402	0	5820	—	—	103	10
Waspaloy	448	183	21	115000	339	0	311	—	—	92	25
IN738 LC	106	−53	109	40500	82	0	445000	134	0	313	2.96
IN738 LC	51	−49	292	46300	230	86.5	318000	—	—	616	5.26

Table 2 Coefficients of the polycrystalline model used for the simulations (units: MPa s)

Material	r_0	Q_1	b_1	Q_2	b_2	D	δ	c	d	k	n
A 316L	31.9	38	10	−19.3	5	61	0.176	1110	0	40	8
Waspaloy	238	47.7	8.1	−17.5	2	28	0.203	1020	0	50	25
IN738 LC	30.2	−28.8	534	0	—	0	—	38100	342	382	9.24

$$\dot{\boldsymbol{\alpha}}_j = \Omega_1' \mathbf{N}\left[1 - \frac{D_j}{C_j}\frac{\mathbf{X}_j : \mathbf{N}}{\mathbf{N} : \mathbf{N}}\right] \quad \text{with} \quad \mathbf{N} \text{ such as } \dot{\mathbf{E}}^p = \Omega_1' \mathbf{N} \tag{6}$$

As is shown in Fig. 5 (dotted line), the biaxial ratchetting is greatly reduced with this rule but the negative ratchetting after removing the axial stress is too important.

4 Comparisons with Experimental Data

4.1 *Methodology*

A significant evaluation of the respective capabilities of these two approaches has to be made on a large experimental database. From a practical point of view, it is first necessary to identify all the material parameters. As the number of material parameters is large (10 or 20 for the studied models), the identification is a difficult task. The method used consists in considering all the expertimental

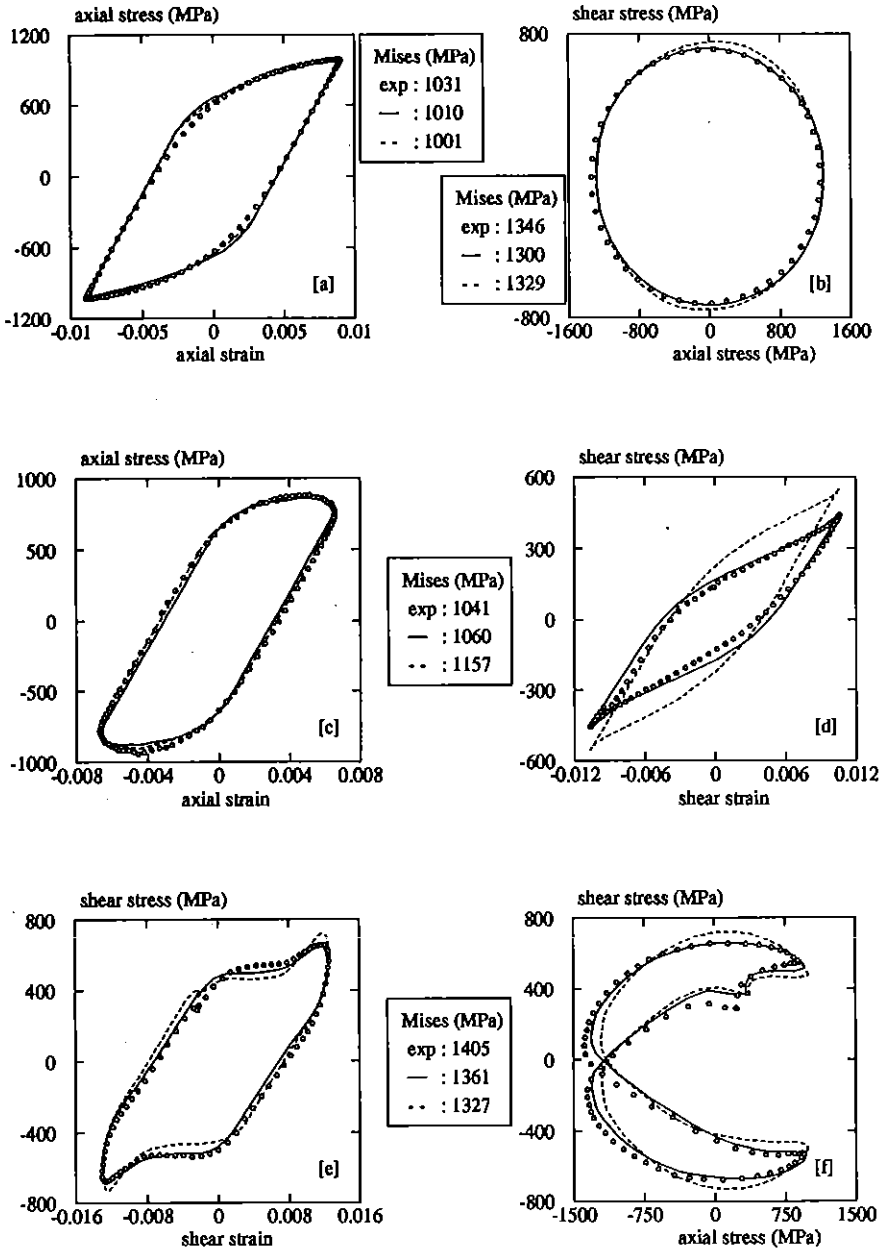

Fig 6 Comparison models *vs* experiments for Waspaloy alloy (at room temperature): (a) tension–compression test; (b) tension–compression/torsion out-of-phase test ($\lambda = 1$, $\phi = 90°$); (c) tension–compression/torsion test ($\lambda = 1$, $\phi = 30°$), axial components; (d) tension–compression/torsion test ($\lambda = 1$, $\phi = 30°$), shear components; (e) tension–compression/torsion butterfly test, axial components; (f) tension–compression/torsion butterfly test, shear components.

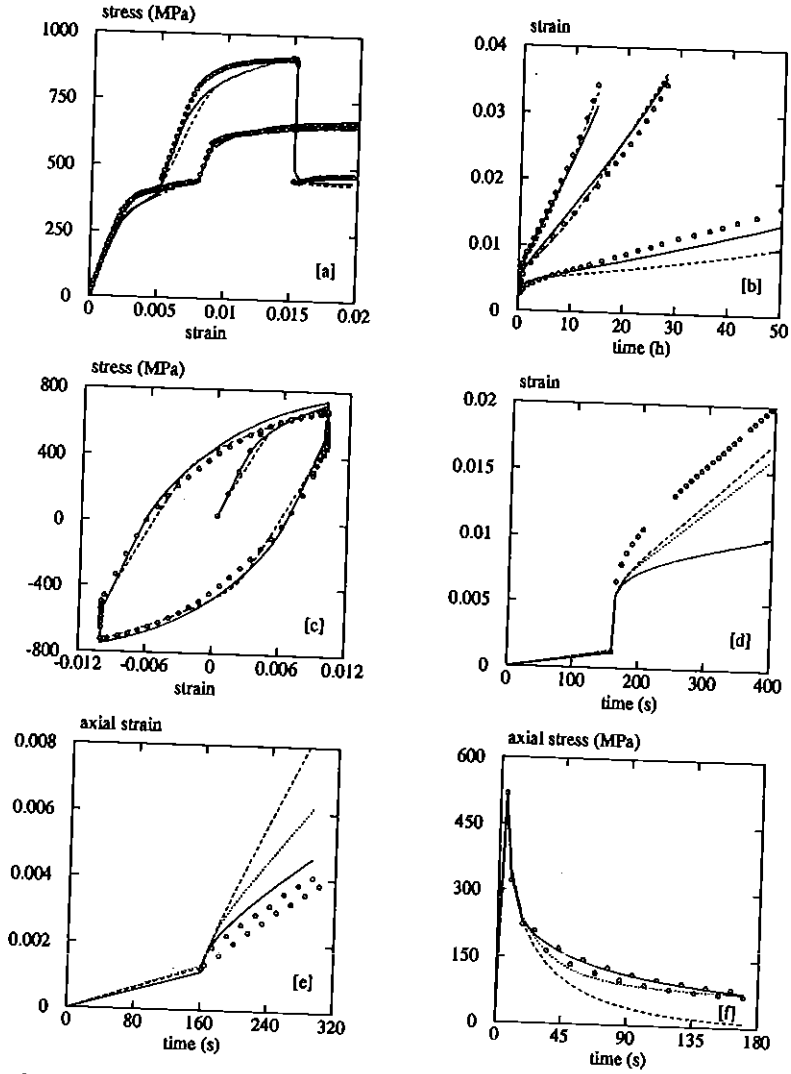

Fig 7 Comparison models *vs* experiments for IN738 LC alloy (at 850°C): (a) tension tests with various strain rates (10^{-6} s^{-1} to 10^{-2} s^{-1}); (b) creep tests (335 MPa, 392 MPa and 410 MPa); (c) fatigue–relaxation test under strain control (strain rate: 10^{-3} s^{-1}, hold time: 30 s); (d) one-dimensional ratchetting test Σ_{min}: 175 MPa, Σ_{max}: 600 MPa, stress rate: 100 MPa s^{-1}); (e) two-dimensional test (Σ_{11}: 175 MPa, $E_{12} = \pm 0.4\%$, period: 17 s); (f) biaxial relaxation test under strain control (E_{11}: 0.4%, $E_{12} = \pm 0.4\%$, period: 17 s).

data and carrying out a simultaneous identification of all parameters with an optimization code (34).

With this systematic method, some difficulties could arise, especially when the model is not good enough to quantitatively describe the set of experiments.

In this case, the difficulty is reduced by eliminating some experimental results. This elimination corresponds implicitly to a reduction of the validity domain of the model. The approach is made on two nickel-base alloys: the first at room temperature for studying time-independent plastic behaviour (Waspaloy) and the second one at 850°C, for studying time-dependent plastic behaviour (IN738 LC).

4.2 *Waspaloy alloy*

This experimental database consists of in-phase and out-of-phase tension–torsion experiments, allowing characterization of the overstrengthening effect (**35**). The most interesting experimental aspect was to exhibit, for this material, a non-proportional strain path which produces more extra-hardening than the classical out-of-phase test with 90° phase lag ($\lambda = 1$, $\phi = 90°$). This loading may be represented by a 'butterfly' in the strain plane, as: $E_{11} = \varepsilon_0 \sin\{2\omega t\}$ and $2E_{12} = \sqrt{3}\varepsilon_0 \sin\{\omega t\}$). The identification of the micromechanical model was performed simultaneously on four tests (tension–compression, two tests with $\lambda = 1$ ($\phi = 30°$ or $\phi = 90°$), and a 'butterfly test'. On the other hand, due to the difficulties mentioned in Section 4.1, the identification of the classical model has been made on two tests only (tension–compression, and the out-of-phase test, $\lambda = 1$, $\phi = 90°$). It has to be noted also that the version of the kinematic hardening rule with a limitation of biaxial ratchetting (**33**) was needed for a correct modelling of the out-of-phase test. The comparison between the models and the experiments is shown in Fig. 6a–f (dashed lines for classical model, solid lines for polycrystalline model), using the coefficients reported in Tables 1 and 2 (using $E = 218$ GPa, $\nu = 0.34$ and, for the polycrystalline model, $a = 1$ and a simple interaction matrix, with $h_{rs} = 1$ and $h_{LC} = 1.41$). Only the polycrystalline model is able to describe the extra-hardening due to the 'butterfly' test.

4.2 *IN738 LC alloy*

An enormous experimental database was made by BAM (**36**) on this material (tension tests, creep, relaxation, uniaxial and biaxial cyclic loading). Twenty tests performed at 850°C were considered for the identification of the models. For this temperature, there is no extra-hardening, so that the basic model in equation (2) can be used, but a non zero recovery potential Ω_2 is needed, allowing the hardening to vanish versus time. As the experimental database is very large, three kinematic variables (two with a non-linear rule (subscripts 1 and 2) and one with Prager's rule (subscript 3)) and one isotropic variable are chosen for the classical model (**5**). The recovery potential Ω_2 is defined in equations (7). The comparison between the models and the experiments is shown in Fig. 7a–f (dashed lines for classical model (NLK), dotted lines (only in Fig. 7d–f) for classical model with a threshold in the nonlinear kinematic rule (*NLK* + *T*),

solid lines for polycrystalline model). For the classical models, the coefficients are reported in Table 1 ($E = 149\,650$ MPa, $\nu = 0.33$) and ($C_3 = 684$ MPa, $m = 9.37$, $M_1 = 736$ MPa $s^{1/m}$ and $M_2 = 887$ MPa $s^{1/m}$ for NLK model) or ($C_3 = 970$ MPa, $m = 12.5$, $M_1 = 600$ MPa $s^{1/m}$ and $M_2 = 575$ MPa $s^{1/m}$ for $NLK + T$ model)

$$\Omega_2(\mathbf{X}_1, \mathbf{X}_2) = \frac{M_1}{m+1}\left[\frac{1}{M_1} J_2(\mathbf{X}_1)\right]^{m+1} + \frac{M_2}{m+1}\left[\frac{1}{M_2} J_2(\mathbf{X}_2)\right]^{m+1} \tag{7}$$

For the polycrystalline model, only ten coefficients reported in Table 2 are used for the identification (with $m = 9.79$ and $M = 298$ MPa $s^{1/m}$). As shown in Fig. 7d, the one-dimensional ratchetting effect is underpredicted for the polycrystalline model. This difficulty might be due at least in part to the use of a simple power function for the viscous stress. For the classical models, the use of a nonlinear kinematic rule with a threshold improves slightly the description of the two dimensional ratchetting test (Fig. 7e) but permits a good prediction of the biaxial relaxation test (Fig. 7f).

5 Conclusion

The comparisons between the simulations and the experiments reported in this paper clearly show that, even using a simplified description of the microstructure, the polycrystalline approaches have better modelling capabilities than inductive approaches. They give a better description and offer better predictions. An additional advantage of the micromechanical models is that they introduce variables which can be explained (or indirectly measured) on a microstructural scale. That makes the dialogue between metallurgy and mechanics easier and provides an assistance for the parameter identification. The large number of variables in these models is a strong limitation for the use in structural computations problems, but they could at least be used as reference solutions for the development and the validation of simplified models. The same idea seems to promote the multimechanisms and multicriteria character of the polycrystalline approaches, even for simplified models. It is then not surprising to observe that the recent developments of the classical approaches follow in some way this requirement, by introducing a larger number of variables to describe hardening, with successive thresholds in the evolution laws.

Acknowledgements

The author is deeply grateful to Drs J. Olschewski and J. Ziebs (BAM, Berlin) for their kindness in providing their experimental data. The author also wants to thank Pr. G. Cailletaud (Ecole des Mines, Paris) for critically reading the manuscript.

References

(1) IKEGAMI, K. (1977) Experimental plasticity on the anisotropy of metals, *Mechanical Behaviour of Anisotropic Solids*, (Edited by J. P. Boehler), CNRS-Euromech 115, Villars de Lans.

(2) PHILIPS, A. (1986) A review of quasistatic experimental plasticity and viscoplasticity, *Int. J. Plasticity*, **2**, 315.

(3) HALPHEN, B., SON, N. Q. (1975) Sur les materiaux standards généralisés, *J. Méca.*, **14**, 39.

(4) BOUCHER, M., CORDEBOIS, J. P. (1994) Incremental evolution of induced anisotropy, *Int. J. Plasticity*, **10**, 909.

(5) CHABOCHE, J. L. (1989) Constitutive equations for cyclic plasticity and cyclic viscoplasticity, *Int. J. Plasticity*, **5**, 247.

(6) VALANIS, K. C. (1980) Fundamental consequences of a new intrinsic time measure plasticity as a limit of the endochronic theory, *Arch Mech.*, **32**, 171.

(7) KREMPL, E. (1975) On the interaction of rate and history dependence in structural metals, *Acta Mech.*, **22**, 53.

(8) OHNO, N., KACHI, Y. (1986) Constitutive model of cyclic plasticity for nonlinear hardening materials, *J. Applied Mech.*, **53**, 395.

(9) GERMAIN, P. (1972) *Cours de mecanique des milieux continus*, Masson, Paris.

(10) LADEVEZE, P., ROUGEE, P. (1989) Plasticité et viscoplasticité sous chargement cyclique – propriétés du cycle limite, *CRAS Paris*, **301**, Serie II (13).

(11) CHABOCHE, J. L. (1991) On some modifications of kinematic hardening to improve the description of ratchetting effects, *Int. J. Plasticity*, **7**, 661.

(12) OHNO, N., WANG, J. D. (1993) Kinematic hardening rules with critical state of dynamic recovery, Part I: Formulation and basic features for ratchetting behaviour, *Int. J. Plast.*, **9**, 375.

(13) LAMBA, H. S., SIDEBOTTOM, O. M. (1978) Cyclic plasticity for nonproportional paths, *J. of Eng. Mat. Tech.*, **100**, 96.

(14) McDOWELL, D. L. (1985) A two surface model for transient nonproportional cyclic plasticity, Part 1: Development of appropriate equations, *J. Applied Mech.*, **52**, 298.

(15) BENALLAL, A., MARQUIS, D. (1987) Constitutive equations for nonproportional cyclic elastoviscoplasticity, *J. of Eng. Mat. Tech.*, **109**, 326.

(16) TAYLOR, G. I. (1938) Plastic strain in metals, *J. Inst. Metals*, **62**, 307.

(17) ZARKA, J. (1973) Etude du comportement des monocristaux métalliques: Application à la traction au monocristal C.F.C., *J. Méca.*, **12**, 275.

(18) HESS, F. (1993) Anisotropic strain hardening in polycrystalline copper and aluminium, *Int. J. Plasticity*, **9**, 405.

(19) CAILLETAUD, G. (1988) Approache micromécanique phénoménologique du comportement inélastique des métaux, *Rev. Phys. Appliquée*, **23**, 353.

(20) BERVEILLER, M., MULLER, D., KRATOCHVIL, J. (1993) Nonlocal versus local elastoplastic behaviour of heterogeneous materials, *Int. J. Plasticity*, **9**, 633.

(21) ZAOUI, A., RAPHANEL, J. L., On the nature of the intergranular accommodation in the modeling of elastoviscoplastic behavior of polycrystalline aggregates, *Proc. of Mécamat '91*, Fontainebleau, Aug 1991, pp. 185–192.

(22) BATDORF, S. B., BUDIANSKY, B. (1949) *A mathematical theory of plasticity based on the concept of slip*, NACA, TN–1871.

(23) LIN, T. H. (1957) Analysis of elastic and plastic strain of FCC crystal, *J. Mech. Phys. Solids*, **5**, 143.

(24) KRONER, E. (1961) Zur plastischen verformung des vielkristalls, *Acta Met.*, **9**, 155.

(25) BERADAI, C., BERVEILLER, M., LIPINSKI, P. (1987) Plasticity of metallic polycrystals under complex loading, *Int. J. Plasticity*, **3**, 143.

(26) ZAOUI, A. (1972) Effets de la désorientation des grains sur le comportement viscoplastique des polycristaux C.F.C., *Int. J. Solids Structures*, **8**, 1089.

(27) HILL, R. (1965) Continuum mechanics of elastroplastic polycrystals, *J. Mech. Phys. Solids*, **13**, 89.

(28) BERVEILLER, M., ZAOUI, A. (1979) An extension of the self-consistent scheme to plastically flowing polycrystals, *J. Mech. Phys. Solids*, **26**, 325.

(29) CAILLETAUD, G. (1992) A micromechanical approach to inelastic behaviour of metals, *Int. J. Plasticity*, **8**, 55.

(30) PILVIN, P., CAILLETAUD, G., Intergranular and transgranular hardening in viscoplasticity,

Proc. IUTAM Creep in structures IV, Cracow, 10–14 Sept. 1990, pp. 171–178.

(31) HAUTEFEUILLE, L., CLAVEL, M., PILVIN, P., CAILLETAUD, G., Mechanical and microstructural modelling under multiaxial loading: Application to 2024 alloy and to Waspaloy, *Proc. of Mécamat* '92, Cachan (France), 1–4 Sept. 1992, pp. 73–98.

(32) CHABOCHE, J. L., NOUAILHAS, D. (1989) Constitutive modeling of ratchetting effects, Part I and II, *J. Engng. Mat. Tech.*, **111**, 384.

(33) BURLET, H., CAILLETAUD, G., Modeling of cyclic plasticity in finite element codes, *Proc. of 2nd Int. Conf. on Constitutive Laws for Engineering Materials: Theory and Applications*, Tucson, Jan. 1987, pp. 1157–1164.

(34) PILVIN, P., Identification des paramétres de modéles de comportement, *Proc. of Mécamat* '88, Besançon (France), Sept. 1988, pp. 155–164.

(35) CLAVEL, M., PILVIN, P., RAHOUADJ, R. (1989) Analyse microstructurale de la deformation plastique sous sollicitations non proportionnelles dans un alliage base nickel, *CRAS Paris*, **309**, (II), 689.

(36) ZIEBS, J., MEERSMANN, J., KUHN, H. J., Effects of proportional and nonproportional straining sequences on hardening/softening behaviour of IN738 LC at elevated temperatures, *Proc. of Mécamat* '92, Cachan (France), 1–4 Sept. 1992, pp. 224–255.